

Evaluation of a Candidate Trace Contaminant Control Subsystem Architecture: The High Velocity, Low Aspect Ratio (HVLA) Adsorption Process

Matthew J. Kayatin[1] and Jay L. Perry[2]
NASA George C. Marshall Space Flight Center, Huntsville, Alabama 35812, USA

Traditional gas-phase trace contaminant control adsorption process flow is constrained as required to maintain high contaminant single-pass adsorption efficiency. Specifically, the bed superficial velocity is controlled to limit the adsorption mass-transfer zone length relative to the physical adsorption bed; this is aided by traditional high-aspect ratio bed design. Through operation in this manner, most contaminants, including those with relatively high potential energy are readily adsorbed. A consequence of this operational approach, however, is a limited available operational flow margin. By considering a paradigm shift in adsorption architecture design and operations, in which flows of high superficial velocity are treated by low-aspect ratio sorbent beds, the range of well-adsorbed contaminants becomes limited, but the process flow is increased such that contaminant leaks or emerging contaminants of interest may be effectively controlled. To this end, the high velocity, low aspect ratio (HVLA) adsorption process architecture was demonstrated against a trace contaminant load representative of the International Space Station atmosphere. Two HVLA concept packaging designs (linear flow and radial flow) were tested. The performance of each design was evaluated and compared against computer simulation. Utilizing the HVLA process, long and sustained control of heavy organic contaminants was demonstrated.

Nomenclature

ACFB	=	Adsorbent Cartridge Fixed Bed
AR	=	atmosphere revitalization
ARREM	=	Atmosphere Resource Recovery and Environmental Monitoring
D3	=	hexamethylcyclotrisiloxane
DCM	=	methylene chloride (dichloromethane)
HVLA	=	high velocity, low aspect ratio
ISS	=	International Space Station
LVHA	=	low velocity, high aspect ratio
NASA	=	National Aeronautics and Space Administration
MSFC	=	Marshall Space Flight Center
TCCS	=	trace contaminant control system
VMS	=	volatile methyl siloxanes
VOC	=	volatile organic compound
A_i	=	adsorption potential energy of species *i*
c_i	=	concentration of species *i*
cm	=	centimeter
C_v	=	heat capacity at constant volume
D_i	=	molecular diffusivity of species *i*
d_p	=	effective particle diameter
ft	=	foot
g	=	gram
G	=	Gibbs free energy

[1]Aerospace Engineer, ECLS Systems, Space Systems Dept., NASA Marshall Space Flight Center/ES62.
[2]Lead Aerospace Engineer, ECLS Systems, Space Systems Dept., NASA Marshall Space Flight Center/ES62.

h = hour
H = enthalpy
in = inch
K = Kelvin
lb = pound mass
L_{ads} = mass transfer zone length
m = meter
min = minute
mL = milliliter
mm = millimeter
mol = mole
N = number of moles of gas adsorbed
P_s^* = saturation vapor pressure
Pe = Péclet number
q = adsorption capacity
R = gas constant
s = second
S = entropy
Sc = Schmidt number
T = temperature
u = fluid velocity
U = internal energy
V = system volume
V_m = molar volume
δ = characteristic length
ε = Polanyi adsorption potential
η = single pass adsorption efficiency
μL = microliter
υ = kinematic viscosity
φ = sphericity

I. Introduction

HISTORICALLY trace contaminant control system (TCCS) adsorption bed design has focused on high aspect ratio (i.e. > 1), low flowrate beds containing granular activated charcoal. Currently aboard the International Space Station (ISS) U.S. Segment, cabin air is purified via a fixed bed containing 22.7 kg (50 lb) of 10 wt. % phosphoric acid-impregnated activated charcoal bed operating at a flow rate of approximately 15.3 m^3/h (9.0 standard ft^3/min). The aspect ratio (bed length/bed diameter) has an order magnitude of approximately two. Operation of adsorption beds in this low flow, high aspect ratio regime is advantageous towards maximizing the bed's single-pass adsorption efficiency as well as ensuring the mass-transfer zone remains relatively shallow, thus maximizing utilization of bed's charcoal adsorption capacity and maximizing bed service lifetime.

The reliability and performance of the current ISS TCCS architecture stands-alone. Recent trends in cabin air-quality, however, have raised the need to investigate and evaluate supplementary or hybrid TCCS architecture designs to further mitigate risk for exploration-class missions. Particular interest has been paid to the emerging class of silicone based contaminants known as volatile methyl siloxanes (VMS), although treatment of high cabin air flowrates is also advantageous for controlling accidental leaks and spills as well protecting process equipment such as condensing heat exchangers from chemically-induced fouling. The extent of VMS impact and range of potential sources, stemming from material offgassing to personal care products, are well described by Perry and Kayatin (2017).[1]

One alternative TCCS functional layout under evaluation for exploration missions sheds current architecture design logic in maintaining thin adsorption zone lengths within charcoal beds. This TCCS architecture, included in the atmosphere revitalization (AR) process depicted by Fig. 1, consists of three components—a high velocity, low aspect ratio (HVLA) adsorbent bed; a low velocity, high aspect ratio (LVHA) adsorbent bed; and a catalytic oxidation process.[2, 3] Components employing HVLA characteristics have previously been deployed aboard the ISS Node 1 to support trace contaminant control during the station's early assembly stages.[4] More recently, the earlier Node 1 HVLA

bed components were adapted toward cabin VMS concentration reduction aboard the ISS.[5] As well, HVLA components have been incorporated in the National Aeronautics and Space Administration's (NASA) exploration mission AR architecture developmental testing.[6]

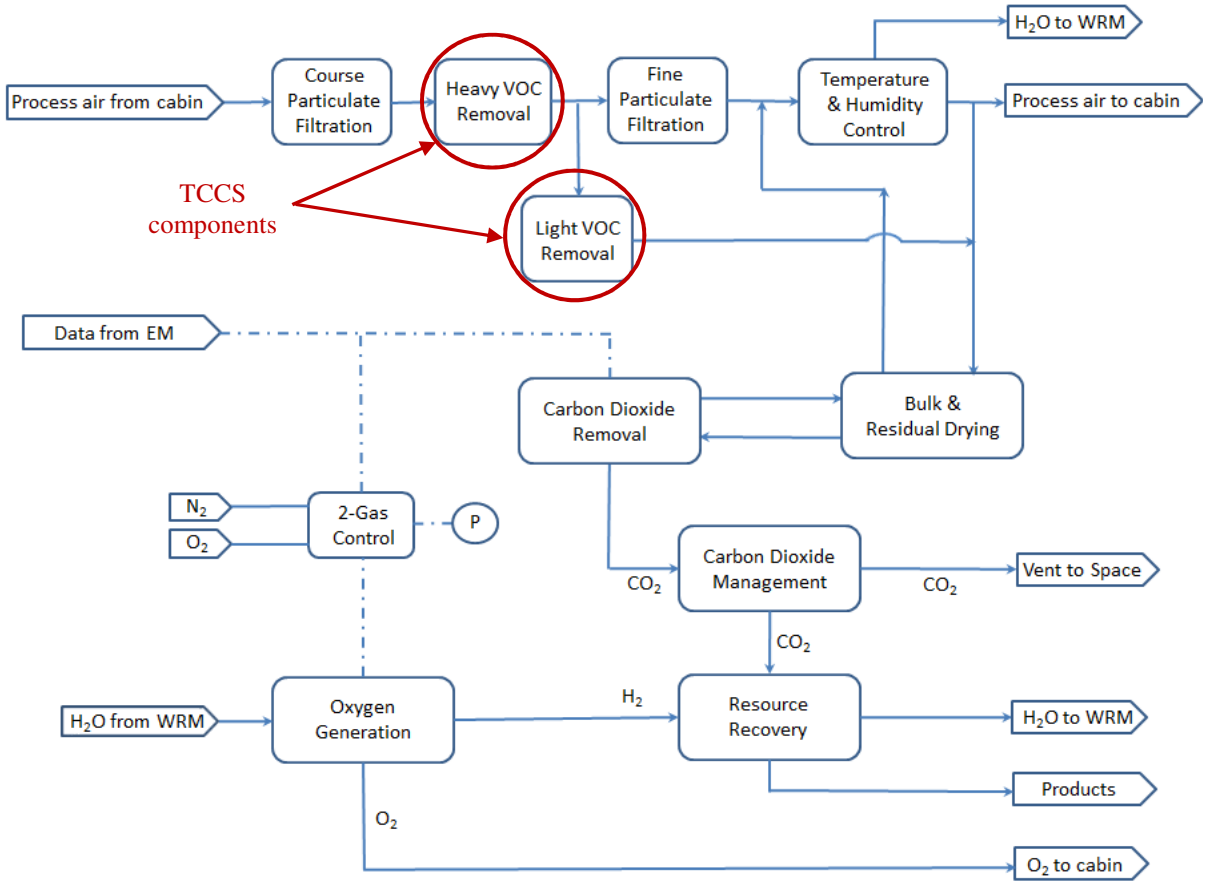

Figure 1. An AR subsystem simplified block diagram for exploration missions. *The TCCS process components are circled in red. The heavy volatile organic compound (VOC) removal process accounts for the HVLA adsorbent bed component. The light VOC removal process accounts for the LVHA adsorbent bed and catalytic oxidation components.*

In the process architecture depicted by Fig. 1, the HVLA component treats relatively high velocity process flowrates >85 m^3/h (>50 standard ft^3/min) with shallow or low aspect ratio absorption beds (i.e. < 1). By operation in this manner, one allows near immediate breakthrough of light or volatile compounds by stretching the length of the theoretical mass transfer zone past that of the physical adsorption bed depth. Within the construct of classic adsorption bed design, this operational approach is nonsensical if the bed is to stand alone within the cabin TCCS. Yet, when the design is considered to supplement a classic LVHA bed the system design logic can be rationalized by considering a limited range of trace contaminant control tasks being asked of the HVLA component in the system. Physically, the high velocity through the HVLA bed imposes a kinetic limitation on the equilibrium adsorption behavior of the activated charcoal. In theory, compounds having sufficiently low potential energy, such as those possessing large molar volumes (V_m) or low vapor pressures (P_s^*), may still be effectively adsorbed even at relatively high superficial velocities. Ground testing at NASA's Marshall Space Flight Center (MSFC) supports this phenomenon.

This operational scenario effectively enables chemical separation by adsorption potential energy (A_i), as described by Polanyi[7] and refined by Dubinin[8], wherein compounds not-readily or weakly adsorbed are either immediately passed downstream or subsequently rolled-off (desorbed) from the bed by more strongly adsorbed compounds over time.[9, 10] The operational logic behind such an approach is two-fold: first, high cabin turnover rates can be realized to treat accidental leaks or problematic compounds of appropriate A_i and second, the available adsorption capacity of the HVLA bed charcoal can be maximized by pushing off high A_i compounds, of which charcoal has an inherently low specific adsorption capacity to contain.

In order to proceed with a detailed design of the TCCS architecture depicted by Fig. 1, theoretical and experimental studies are required to characterize the behavior of various HVLA adsorption bed designs. Furthermore, a theoretical construct to classify the partitioning of compounds by A_i as a function of process conditions is absent. A consequence of operation within the HVLA adsorption operational regime is the potential for the HVLA bed to become a generation source for high A_i compounds over time; this is a situation in which NASA has limited experimental knowledge. Towards this end, the HVLA adsorption process architecture was demonstrated against a trace contaminant load representative of the ISS atmosphere. Two HVLA concept packaging designs (linear flow and radial flow) were tested. The performance of each design was evaluated and compared against computer simulation. Performance data and lessons learned are highlighted within.

II. Adsorption Potential Theory

The adsorption potential energy can be derived from classical thermodynamics by the definition of the Gibbs free energy (G) as shown by Eq. 1. Here G is defined in terms of the enthalpy (H) and entropy (S) at thermodynamic temperature (T). The enthalpy, H, can be further described in terms of internal energy (U), system pressure (P), and system volume (V).

$$G \equiv H - TS = (U + PV) - TS \tag{1}$$

Taking the finite differentials of Eq. 1 in accordance with the chain rule, yields Eqs. 2 and 3.

$$dG = d(U + PV) - d(TS) \tag{2}$$

$$dG = dU + PdV + VdP - SdT - TdS \tag{3}$$

Stating the first law of thermodynamics in terms of an ideal gas yields Eq. 4 where C_v is the constant volume heat capacity.

$$dU = C_v dT = dq - PdV \tag{4}$$

If the adsorption occurs reversibly then statements in Eq. 5 and Eq. 6 are true and we arrive at Eq. 7.[11]

$$dq_{rev} = TdS \tag{5}$$

$$P_{ext} = P_{sys} \tag{6}$$

$$dU = TdS - PdV \tag{7}$$

Inserting Eq. 7 into Eq. 3 and reducing terms results in the following expression for dG (Eq. 8) which reduces to Eq. 9 for an isothermal process as described by Polanyi.

$$dG = VdP - SdT \tag{8}$$

$$dG = VdP \tag{9}$$

For N moles of an ideal gas adsorbed, its volume can be related to its pressure via the gas constant R as shown by comparison between Eq. 9 and Eq. 10.

$$dG = \frac{NRT}{P} dP \tag{10}$$

Integration of Eq. 10 with respect to P yields Eq. 11.

$$\Delta G = NRT\ ln\frac{P_2}{P_1} \tag{11}$$

The resulting relationship for the Gibbs free energy matching the general form of the Polanyi potential (ε) indicates that it is a description of the isothermal work of compression upon adsorption of a molecule from the vapor phase at equilibrium pressure P_1 to the saturation pressure (liquid state) at P_2.[12] A sign convention can be interpreted from the physical situation being described via the pressure ratio. Note this theory does not propose a predictive relationship for the "characteristic curve" relating the adsorption potential with amount adsorbed. As such, the adsorption potential approach can be considered a phenomenological framework characteristic of the sorbent itself and therefore must be experimentally measured. The adsorption capacity (q) can therefore be related to the potential by some arbitrary functional form as displayed by Eq. 12.

$$q = f[\varepsilon] = f\left[RT\ ln\frac{P_2}{P_1}\right] \tag{12}$$

A discussion of various forms of ε relevant to TCCS design can be found in Perry (1998).[13] As is convention in historical spacecraft adsorption bed design, the working form of ε is given by Eq. 13 and scaled by the product of N and the molar volume at normal boiling point (V_m).[8, 13] Here the adsorption potential for component i (A_i) is found by the logarithm of the saturation pressure (P_s) to partial pressure (P_i) ratio. Recent discussion on design methodology and equipment sizing based on adsorption potential regression is provided in Monje et al. (2016).[14]

$$\varepsilon = A_i = \frac{T}{V_m} \log_{10}\left(\frac{P_s}{P_i}\right) \tag{13}$$

III. Experimental HVLA Architecture Testing

The HVLA component testing was conducted in the MSFC Environmental Chamber testing facility. This facility consists of a 90.6 m^3 (3200 ft^3) chamber outfitted with test support equipment to inject trace chemical contaminants; to provide chamber ventilation, temperature, and humidity control; to provide chamber atmospheric pressure control; to simulate human metabolic loads and demands; and to monitor the chamber's internal conditions. Additional details on the Environmental Chamber facility can be found in Ref. 15. Two HVLA configurations were evaluated that employed different process air flow patterns—an axial flow cartridge with flat adsorbent-filled panels arranged in a "V" configuration and a radial flow cartridge. The HVLA test articles and testing methods are described and experimental results are summarized by the following sections.

A. HVLA Test Articles

The following describes the axial flow and radial flow HVLA test articles and summarize the flow conditions for each testing series.

1. Axial Flow Cartridge Architecture

The axial flow cartridge architecture, also known as the adsorbent cartridge fixed bed (ACFB) assembly (Calgon Carbons, Barnabey Sutcliffe Division, BSC/062418), is a candidate HVLA architecture evaluated during a series of integrated tests conducted by MSFC for the Atmosphere Resource Recovery and Environmental Monitoring (ARREM) project which was sponsored by the NASA Advanced Exploration Systems (AES) Program.[15] Figure 2 displays a single ACFB assembly cartridge, its nominal dimensions, and the process air flow path. The cartridges were of high-impact polystyrene construction. Based on the geometry of the ACFB cartridge, the process air flow exposed to the actual charcoal bed depth is of unknown distribution. Testing was conducted within the MSFC Environmental Chamber during Phase 4 of ARREM Cycle 2 testing. The ACFB assembly consisted of three vertically stacked activated carbon cartridges arranged in parallel just upstream of the cabin ventilation fan. In this arrangement, the full cabin ventilation flow of approximately 850 m^3/h (500 ft^3/min) was drawn through the ACFB assembly. This flow is comparable to the 680 m^3/h (400 ft^3/min) total ventilation flow provided by the ISS laboratory module cabin fan. The ACFB cartridges were packed with ~24.5 kg (54 lb) of a candidate 4 x 8 mesh granular adsorbent media (Ammonasorb II, Calgon Carbons). Additional details pertaining to the ACFB are provided in Perry et al. (2015).[15]

Figure 2. Calgon axial flow HVLA cartridge architecture and flow path. *Nominal cartridge dimensions are 6 in high × 24 in wide × 18 in deep. Three cartridges were installed in parallel during testing.*

2. Radial Flow Cartridge Architecture

A radial flow HVLA adsorption architecture, shown by Fig. 3, containing eight parallel flow hollow-cylinder charcoal adsorption beds was studied in hope that the well-defined 2.54 cm (1 in) deep

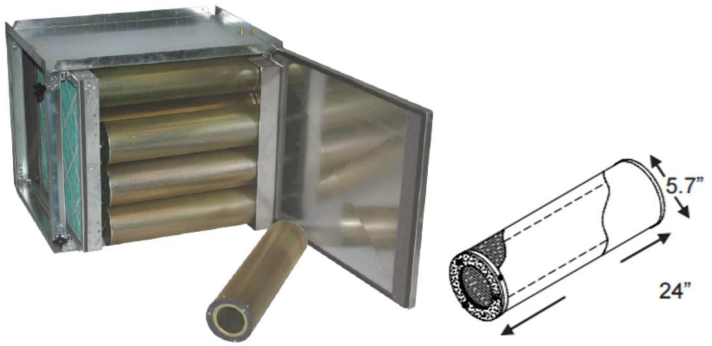

Figure 3. Camfil radial flow HVLA housing architecture and nominal cartridge dimensions (in). *Eight cartridges were installed in the housing.*

flow path would improve process performance and predictability for computer modelling and TCCS design considerations. The cartridge enclosure depicted in Fig. 3 was manufactured by Camfil (GP-SMH-A-1X.5) and features an insulated, aluminized construction. Each of the eight individual CamCarb charcoal canisters (CC-CG35) was of plastic construction and filled with Camfil's untreated, grade CEX004 activated carbon pellets (4 mm diameter × random chopped length). Measurements at MSFC indicate that these chopped cylinders have a diameter of 0.41 ± 0.02 cm (0.16 in) and bimodal length distribution having means of 0.53 cm (0.21 in) and 0.81 cm (0.32 in). For the purpose of hydrodynamic analysis herein, the geometric length mean of 0.66 cm ± 0.20 cm (0.26 in) was used in conjunction with the measured diameter to determine an effective spherical diameter (d_p). The particle sphericity (φ) was calculated as a ratio of sphere to cylinder surface areas of equivalent particle volume (8.65E-02 cm^3) and found to be 0.85.[16] The effective particle size was determined by the product of φ and d_p sphere and found as 0.47 cm (0.185 in). Figure 3 shows the cylinder arrangement and flow path of the system. Process flow is drawn through the prefilter and into the inner canister diameters. The canisters have a nominal outside diameter of 14.5 cm (5.7 in) and are 61 cm (24 in) long with a packed volume of approximately 5233 cm^3 (319 in^3). The packed volume for eight cartridges accommodated approximately 20.1 kg (44.4 lb) of the activated carbon pellets which is within twenty percent of the axial flow ACFB cartridge carbon mass. The entire enclosure was attached to the Environmental Chamber's underfloor ventilation duct in the same manner as the ACFB. As with the ACFB, the full ventilation flow of 850 m^3/h (500 ft^3/min) was drawn through the radial flow cartridge test article.

B. Analytical Methods

Chemical analysis was performed with an Agilent 7890 capillary gas chromatograph (GC) utilizing a single analytical column [Restek Rxi-624Sil MS (20 m x 0.18 mm x 1.0 µm)] equipped with both a flame ionization and mass selective detector. A Gerstel TDSG thermal desorption system provided cryogenic (-120 °C) trapping of contaminants on quartz glass wool at the GC inlet and metered sample flows using an integrated mass flow controller. Calibrations were made using gas phase standards generated via National Institute for Standards and Technology traceable permeation tubes heated within a Kin-Tek gas generator and regulated by a Kin-Tek Interface Module. Calibrations were referenced to the flame ionization detector whereas the mass selective detector was utilized for identification of chemical unknowns and reaction byproducts. Samples were drawn from the Environmental Chamber in a closed loop utilizing an external sample pump and sample flow was provided via slip stream to the GC and returned via the Gerstel sampling loop to the chamber to avoid any mass losses.

C. Contaminant Injection Methods

A chemical challenge representative of trace contaminant load conditions in the ISS cabin was used during HVLA component testing. Contaminants were administered continuously at a rate of 10 µL/min by syringe pump. In order to ensure hexamethylcyclotrisiloxane (D3) dissolution in the cocktails, D3 siloxane was gently stirred in a mixture of the alcohols and acetone only, prior to adding the other liquid contaminants. Injection methods were the same for both component test.

1. Contaminant Injection during Axial Flow Cartridge Testing

Trace contaminants were introduced into the Environmental Chamber by continuously injecting a liquid chemical cocktail into a ventilation recirculation loop of the chamber's main ventilation duct system wherein the chemicals vaporized into the cabin atmosphere. The liquid density of the chemical cocktail was experimentally determined to be 0.81 g/mL. Table 1 lists the chemical cocktail contaminant species and mass injection rates for the ACFB component testing.

2. Contaminant Injection during Radial Flow Cartridge Testing

Similarly to the axial flow ACFB component test, contaminants were continuously injected during the radial flow HVLA cartridge testing and the resulting mass injection rates are highlighted in Table 2. The liquid density of the chemical cocktail was experimentally determined to be 0.83 g/mL, slightly higher than the ACFB test due to the omission

Table 1. Contaminant injection rates for axial flow cartridge testing.

COMPOUND	mg/h
Methanol	44.9
Ethanol	274.0
2-Propanol (Isopropanol)	19.2
Ethanal (Acetaldehyde)	29.8
Xylenes	9.2
DCM (Methylene Chloride)	5.3
2-Propanone (Acetone)	24.7
Trimethylsilanol	9.2*
Hexamethylcyclotrisiloxane	69.6

*Trimethylsilanol reacted with primary alcohols to form derivatives methoxytrimethylsilane and ethoxytrimethylsilane.[17]

Table 2. Contaminant injection rates for radial flow cartridge testing.

COMPOUND	mg/h
Methanol	46.90
Ethanol	286.23
2-Propanol (Isopropanol)	20.05
Ethanal (Acetaldehyde)	31.15
Xylenes	9.67
DCM (Methylene Chloride)	5.55
2-Propanone (Acetone)	25.78
Hexamethylcyclotrisiloxane	72.68

of trimethylsilanol. Trimethylsilanol was not included in this mixture to avoid the reaction with primary alcohols observed during earlier testing.[16]

D. Experimental Results

The performance of HVLA beds was continuously tracked by the single pass adsorption efficiency (η) as described by Eq. 14

$$\eta = \frac{C_{i,in} - C_{i,out}}{C_{i,in}} \times 100\ \% \tag{14}$$

wherein the concentration of species i was measured at the bed inlet and outlet by GC. The following summarizes the test results for each HVLA bed flow configuration.

1. Axial Flow Cartridge Test Results

The axial flow ACFB adsorption test results were reported previously in Perry and Kayatin (2015).[16] These results, shown by Fig. 4, found that the initial measured adsorption efficiency of ethanol was approximately 45 % and decreased below 10 % near the test end. Initially, isopropanol was adsorbed at 95 % efficiency and exhibited breakthrough at a slightly slower rate. Acetone was also initially adsorbed with high efficiency through Test Day 4 but decreased rapidly. Xylene was not detected in the chamber atmosphere during this test phase indicating 100 % efficiency was maintained. D3 siloxane was adsorbed with a mean efficiency of 78 %. Other light compound test data was not shown due to the significant noise which may indicate non-uniform breakthrough and/or flow distributions.

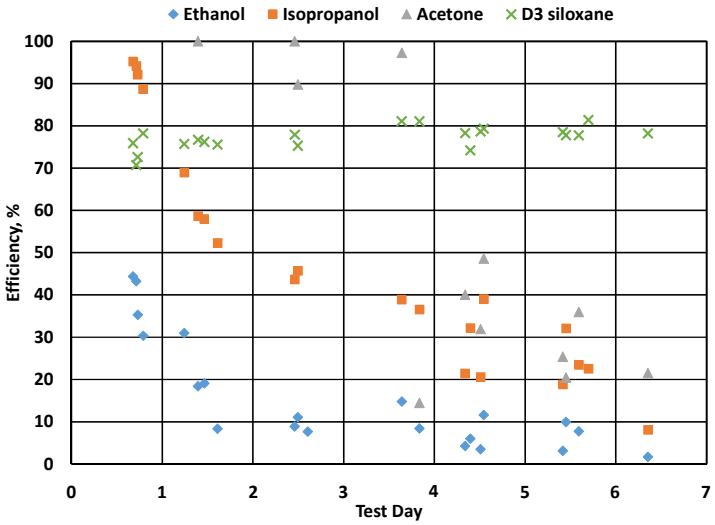

Figure 4. Experimental ACFB single pass adsorption efficiency.

2. Radial Flow Cartridge Test Results

Figure 5 displays the measured single-pass adsorption efficiency for the radial flow HVLA adsorption beds. Volatile compounds (methanol, acetaldehyde, ethanol, and DCM) broke through the radial beds shortly after test start. Acetone and isopropanol breakthrough was slightly delayed. Compounds of low A_i (D3 siloxane and xylene) were effectively controlled over the test duration, and in equivalent magnitude to the ACFB process, demonstrating HVLA performance as intended. Overall, performance was similar to the axial flow cartridge configuration. Data resolution was improved for light compounds, likely indicating a more uniform flow distribution over the ACFB. One notable difference was the negative efficiency observed for light alcohols in the radial configuration. This observation likely indicates light (high A_i) compound roll-off from saturation with heavier (low A_i) compounds and under continued operation the radial beds would serve as a contaminant generation source for these compounds, as hypothesized. The absence

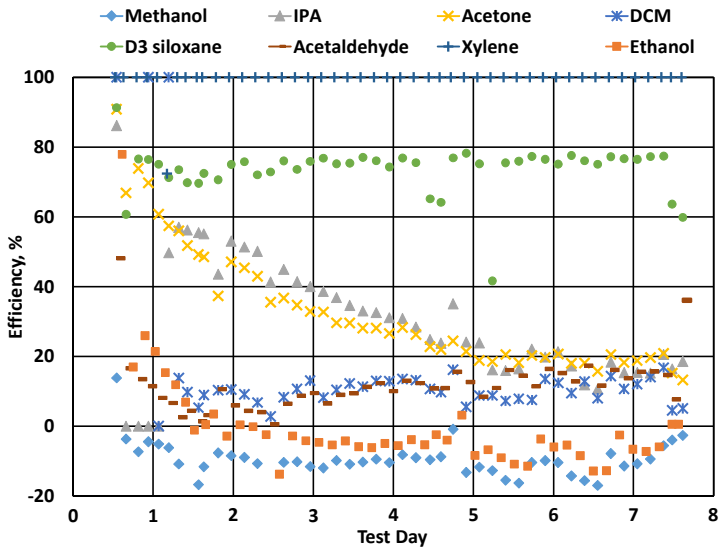

Figure 5. Experimental single pass adsorption efficiency from eight parallel radial flow HVLA adsorption beds.

of observed compound roll-off for the ACFB test may be a result of differences in sorbent capacity between each architecture and/or uneven flow distribution.

Based on these results, efforts towards producing a hierarchical model of HVLA retention based on contaminant physical properties and potential energy was pursued.

IV. Computer Simulation

The TCCS computer simulation is described by NASA TM-108456 and historically has been used for design and performance predictions on traditional low flow, high aspect ratio adsorption beds.[18] The sensitivity of the mass-transfer zone length to process flow rate is empirically based on LVHA test data in the computer model and therefore may be challenged when asked to predict accurate performance for HVLA bed designs.

A. Axial Flow Cartridge Architecture

Each ACFB cartridge is comprised of two rectangular panels having 3.24 cm (1.275 in) sorbent thickness placed in a truncated "V" shape arrangement with the vertex orientated upstream to process flow. Actual cartridge dimensions are 14.13 cm (5.5625 in) high × 57.94 cm (22.8125 in) wide × 43.66 cm (17.1875 in) deep. Looking at the ACFB face normal to upstream process flow, 6.35 cm (2.5 in) of the cartridge height is blocked. Thus, 367.9 cm^2 (57.03 in^2) of the cartridge inlet cross sectional area [818.7 cm^2 (126.9 in^2)] is blocked from flow. It follows that for the complete stack of three ACFB filters, 1352.2 cm^2 (209.6 in^2) of open area is presented to the 850 m^3/h (500 ft^3/min) process flow at the ACFB inlet. Treating the flow as incompressible, the duct inlet velocity can be estimated to be 174.5 cm/s (68.7 in./s). At this fluid velocity, the Mach number was estimated to be 5.1E-03 which supports analytical treatment of the process flows as incompressible (Mach number < 0.3).[16] The rear of a single ACFB unit has 413.9 cm^2 (64.2 in^2) open to exiting air flow which scales to 1241.8 cm^2 (192.5 in^2) for the complete filter stack. Therefore, the duct exit velocity can be estimated to be 190 cm/s (74.8 in/s). The nominal total face area of both panels in each cartridge is 4541.9 cm^2 (704 in^2) of which 4493.64 cm^2 (696.5 in^2) is wetted to the flow. The nominal face area is required for estimating sorbent volume while the wetted area can be used to estimate the adsorption bed velocity. Spreading the entire duct flow over the wetted area for all three filters [13480.9 cm^2 (2089.5 in^2)] results in a bed adsorption velocity of 17.5 cm/s (6.89 in/s).

To maintain compatibility with the simulation input, each of the three ACFB units was modeled as a cylindrical axial flow bed. To preserve bed velocity, the wetted area was used to find an equivalent cylindrical bed diameter of 0.76 m (29.9 in). To preserve total sorbent mass, the nominal single cartridge (2-panel) charcoal volume of 0.0164 m^3 (1003.5 in^3) was used in conjunction with the cylindrical diameter to define an equivalent bed depth of 3.6 cm (1.42 in.). In this manner, the breakthrough of three parallel flow cylindrical beds of 0.76 m diameter and 3.6 cm depth were simulated at a process flow of 283 m^3/h (166.56 ft^3/min) against the contaminant load defined by Table 1. A characteristic adsorption capacity for phosphoric acid treated charcoal was used.[13] Figure 6 displays the simulation results for compounds shown by Figure 4 test data. Remarkably, D3 siloxane and xylene were predicted to maintain high single pass adsorption efficiencies of 91 % and 80 %, respectively. This result is in acceptable agreement with experiment. The breakthrough trends for ethanol also matched very well. Trends for isopropanol were also in general agreement but simulation predicted better control than experimentally found at longer test durations. Acetone, however did not match experimental test data wherein breakthrough was delayed for nearly 4 test days.

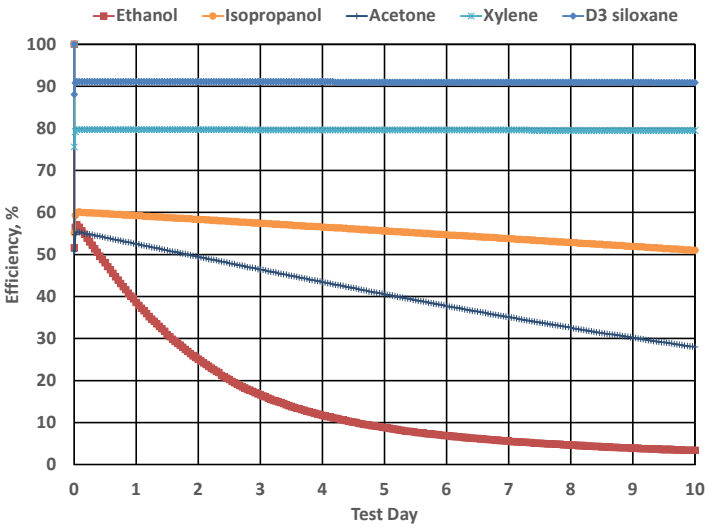

Figure 6. Simulated ACFB single pass adsorption efficiency for three parallel axial flow beds.

B. Radial Flow Cartridge Architecture

Each radial flow cartridge has an outer diameter of 14.35 cm (5.65 in) and inner diameter of 8.08 cm (3.18 in). The plastic cartridge housing occupies approximately 0.125 in of each radii resulting in an actual charcoal bed outer diameter of 13.72 cm (5.4 in) and inner diameter of 8.71 cm (3.43 in). The charcoal bed is 59.37 cm (23.375 in) in length. The adsorption flow path is from inner to outer diameter. Thus, at the duct inlet a cross sectional area of 51.2 cm^2 (7.94 in^2) per cartridge is presented to the 850 m^3/h (500 ft^3/min) process flow. The total open area for eight cartridges is 410 cm^2 (63.5 in^2) which results in a duct inlet velocity of 576 cm/s (227 in/s). Note that at this velocity the Mach number was estimated to be 1.7E-02. Due to the radial flow path, the mid-bed surface area of 2098.8 cm^2 (325.3 in^2) per cartridge was used to estimate the bed adsorption velocity as 14.1 cm/s (5.53 in/s). Therefore, the radial bed velocity is approximately 80 % of the ACFB architecture bed velocity.

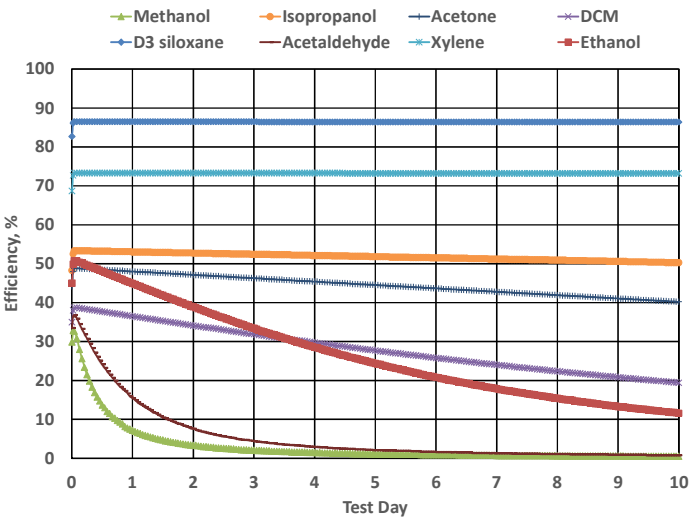

Figure 7. Simulated HVLA single pass adsorption efficiency for eight parallel, radial flow adsorption beds.

The breakthrough profile for eight radial flow, cylindrical beds of 0.594 m (23.375 in) length and operating in parallel were simulated. The beds have an inner diameter of 0.087 m (3.43 in) with outer diameter of 0.137 m (5.40 in) and were challenged at a process flow of 850 m^3/h (500 ft^3/min) against the contaminant load defined by Table 2. A characteristic adsorption capacity for untreated charcoal was used for analysis.[13] Figure 7 displays the simulation results. D3 siloxane and xylene were predicted to maintain high single pass adsorption efficiencies of 87 % and 73 %, respectively. This result was generally in agreement with experiment with better control of xylene observed for both HVLA geometries. Methanol and acetaldehyde broke through almost immediately, in agreement with experiments. Ethanol was predicted to be slightly better controlled than experimentally observed. The predicted control of acetone and isopropanol was better than experiment but, in general, the delayed breakthrough for intermediate A_i compounds were in agreement.

V. Component Separation Criterion

The feasibility of the HVLA adsorption process hinges on the magnitude of the contaminant adsorption work (the potential) being sufficiently small to ensure mass transfer at short sorbent contact times. In accordance with Eq. 13, A_i was found based on the target cabin concentrations utilizing previously published physical properties.[19] Remarkably, as shown by Table 3, the lowest predicted values of A_i were on the order of 1.0E+01 K-mol/mL for both compounds effectively controlled (Xylene and D3 siloxane). The observed and predicted long-duration control for these compounds by both HVLA architectures is a result of their low potential energy and molecular diffusivity.

While the adsorption of compounds having low A_i is consistent with experimental observations, a criterion delineating adsorption vs. breakthrough is unknown. Physically, it may be instructive to examine the relative importance of mass transfer from fluid advection to diffusion in this flow regime as described by the Péclet number (Pe). Equation 15 describes Pe_i in terms of the fluid velocity (u), characteristic length (δ), and molecular diffusivity of compound i (D_i). For the current physical situation, the bed depth can be taken as the characteristic length. The Péclet number can now be interpreted as the ratio of bed velocity to contaminant molecular diffusivity acting over the bed depth.

$$Pe_i = \frac{u\delta}{D_i} \tag{15}$$

Since the bed depth is well defined and flow path is well distributed for the radial flow HVLA architecture, its flow path was be used for estimation of Pe_i. In this case the characteristic length is 2.54 cm. The flow velocity per canister was previously estimated to be 14.1 cm/s (5.53 in/s) at mid-bed depth for the 850 m^3/h (500 ft^3/min) process flow. Recalling the effective particle size of 0.47 cm for the cylindrical sorbent, the particle Reynolds number was found to be 42 which indicates mostly viscous losses within the beds. Table 4 displays the diffusion coefficients and Pe_i for

Table 3. Adsorption potential for trace contaminants at targeted chamber load. *Bold values of A_i and $D_{i\text{-}Air}$ indicate compounds controlled by HVLA adsorption processes.*

COMPOUND	mg/m³	P_s^* [mg/m³][19]	V_m [mL/mol][19]	A_i [K-mol/mL]	$D_{i\text{-}Air}$ [cm²/s]
Methanol	0.7	194,708	42.5	38.17	0.165[a]
Ethanol	4.8	127,574	62.1	21.23	0.128[a]
2-Propanol (Isopropanol)	0.4	125,696	80.9	20.25	0.104[a]
Ethanal (Acetaldehyde)	0.6	2,021,809	56.9	34.19	0.173[¥]
Xylene	0.2	38,600[$]	139.5	**11.29**	**0.069**[a]
DCM (Methylene Chloride)	0.1	1,860,277	65.1	33.28	0.104[¥]
2-Propanone (Acetone)	0.5	663,190	77.5	23.54	0.107[a]
Hexamethylcyclotrisiloxane	1.5	51,121	187[#]	**7.22**	**0.052**[¥]

[$]Mean isomer value. [#]At sublimation. [¥]See Appendix for calculations.
[a]Tang, M. J., Shiraiwa, M., Pöschl, U., Cox, R. A., & Kalberer, M. (2015). Compilation and evaluation of gas phase diffusion coefficients of reactive trace gases in the atmosphere: Volume 2. Diffusivities of organic compounds, pressure-normalised mean free paths, and average Knudsen numbers for gas uptake calculations. Atmospheric Chemistry and Physics, 15(10), pp. 5585-5598.

each compound. The calculated values for Pe_i indicate that convective mass transfer dominates for all compounds and thus a well-defined kinetic criterion for adsorption was not apparent, however, observations of $Pe_i > 500$ are consistent with compound control.

Table 4. Diffusion coefficients and calculated Pe_i & Sc_i for trace HVLA contaminants. *Bold values indicate compounds controlled by HVLA adsorption processes.*

COMPOUND	$D_{i\text{-}Air}$ [cm²/s]	Pe_i	Sc_i
Methanol	0.165[a]	216	0.9
Ethanol	0.128[a]	279	1.2
2-Propanol (Isopropanol)	0.104[a]	343	1.5
Ethanal (Acetaldehyde)	0.173[¥]	206	0.9
Xylene	**0.069**[a]	**517**	**2.3**
DCM (Methylene Chloride)	0.104[¥]	343	1.5
2-Propanone (Acetone)	0.107[a]	334	1.5
Hexamethylcyclotrisiloxane	**0.052**[¥]	**686**	**3.0**

[¥]See Appendix for calculation.
a: Tang, M. J., Shiraiwa, M., Pöschl, U., Cox, R. A., & Kalberer, M. (2015). Compilation and evaluation of gas phase diffusion coefficients of reactive trace gases in the atmosphere: Volume 2. Diffusivities of organic compounds, pressure-normalised mean free paths, and average Knudsen numbers for gas uptake calculations. Atmospheric Chemistry and Physics, 15(10), 5585-5598.

der 1.0E+01 K-mol/mL or less may be suitable criterion for this limited dataset.

Highlighted by Table 3, there exists an approximate range of intermediate A_i between 12 - 20 K-mol/mL that is uncharacterized by the testing and analysis herein. Contaminants and/or loads characterizing this gap in A_i must be studied in future HVLA architecture testing to fully capture the transition to breakthrough. Furthermore, results from computer simulations struggled to predict breakthrough trends for compounds within this intermediate A_i range. Recommend contaminants to bridge this gap are 2-butanone (methyl ethyl ketone) and 2-methyl-1-propanol (isobutanol) with a targeted chamber concentration of 1.0 mg/m³. At this load, A_i for 2-butanone and 2-methyl-1-propanol are predicted to be 17.0 K-mol/mL and 13.3 K-mol/mL, respectively.

Similarly, the relative influence of viscous to molecular diffusion in mass transfer operations can be described by the Schmidt number (Sc). Equation 16 describes Sc_i in terms of the kinematic viscosity (ν) and molecular diffusivity of compound i (D_i).

$$Sc_i = \frac{\nu}{D_i} \tag{16}$$

Examining Table 4, it appears that contaminants with $Sc_i > 1.5$ are well controlled by HVLA processes. Additionally, comparison between D_i and A_i for compounds well controlled by HVLA indicate that compounds with D_i of order 5.0E-02 cm²/s and A_i of or-

Table 5. Prediction of adsorption zone length for trace HVLA contaminants. *Bold values indicate compounds controlled by HVLA adsorption processes.*

COMPOUND	L_{ads} [in][¥]
Methanol	0.479
Ethanol	0.266
2-Propanol (Isopropanol)	0.254
Ethanal (Acetaldehyde)	0.429
Xylene	**0.142**
DCM (Methylene Chloride)	0.417
2-Propanone (Acetone)	0.295
Hexamethylcyclotrisiloxane	**0.091**

[¥]L_{ads} evaluated at 14.1 cm/s.

VI. Adsorption Zone Lengths

During the development of the ISS TCCS by Lockheed, adsorption mass transfer zone length (L_{ads}) was correlated with bed superficial velocity as a function of A_i.[9-10,13] Correlations were only studied at low flowrate, in accordance with the original TCCS design, having a bed superficial velocity of 0.66 cm/s. Table 5 displays the predicted adsorption zone lengths provided by this correlation. Extending this correlation two orders of magnitude, to relevant HVLA velocities of approximately 1.0E+01 cm/s, is problematic as evidenced by comparison with test breakthrough data. According to Table 5, all compounds would have been expected to breakthrough, in disagreement with experimental results. It appears that predictions using this correlation at high velocity might be low by a factor of two or three. Uncertainty in this value limits the accuracy of bed design and estimates for hardware service lifetime. Therefore, it further bench-scale testing must be done at relevant velocities in order to enable proper design and lifetime analysis for HVLA adsorption beds.

VII. Conclusion

Two candidate HVLA adsorption process architectures were tested against a trace contaminant load representative of the ISS atmosphere. For both the linear and radial designs tested, effective contaminant control was demonstrated for compounds of low adsorption potential, proving out the proposed TCC operational concept. In spite of the limited flow range basis for mass-transfer zone length correlations, predictions of contaminant breakthrough by computer simulation were generally in agreement with experimental observations, especially for contaminants of either low or high adsorption potential. Areas for improving our understanding of the HVLA adsorption breakthrough threshold, particularly in regard to compounds of intermediate adsorption potential, were also identified for further study. Inclusion of the HVLA adsorption process within future ECLS exploration architectures will help protect sensitive processes and equipment as well as help ensure safe control over onboard contaminant leaks and/or emerging environmental contaminants, lowering risk for exploration-class missions.

Appendix

The diffusion coefficient for D3 siloxane was estimated from critical properties by the method of Wilke and Lee (1955).[a] Critical parameters for D3 siloxane were obtained from Flaningam (1986)[b] and the liquid molar volume at normal boiling point was estimated from the critical volume by the method of Tyn and Calus (1975)[c]. The diffusion coefficients for acetaldehyde and methylene chloride were estimated by the method of Fuller et al. (1966) by utilization of atomic diffusion volumes.[d]

[a]Wilke, C. R., and Lee, C. Y., "Estimation of Diffusion Coefficients for Gases and Vapors," *Industrial & Engineering Chemistry*, Vol. 47, No. 6, 1955, pp. 1253-1257.

[b]Flaningam, O. L. (1986). "Vapor pressures of poly (dimethylsiloxane) oligomers," *Journal of Chemical and engineering Data*, Vol. 31, No. 3, 1986, pp. 266-272.

[c]Tyn, M. T., and Calus, W. F., "Estimating liquid molal volume," *Processing*, Vol. 21, No. 4, 1975, pp. 16-17.

[d]Fuller, E.N., Schettler, P.D. and Giddings, J.C., "New method for prediction of binary gas-phase diffusion coefficients." *Industrial & Engineering Chemistry*, Vol. 58, No. 5, 1966, pp.18-27.

Acknowledgments

The authors acknowledge the AES ARREM project for funding the ACFB testing, the AES Life Support Systems project for funding the radial HVLA testing, and the MSFC Space Systems Department Technical Excellence funding for the radial HVLA procurement.

References

[1]Perry, J.L. and Kayatin, M.J., "The Incidence and Fate of Volatile Methyl Siloxanes in a Crewed Spacecraft Cabin," ICES-2017-233, *47th International Conference on Environmental Systems,* Charleston, South Carolina, 2017.

[2]Howard, D., Perry, J., Sargusingh, M., and Toomarian, N., "Notional Environmental Control and Life Support System Architectures for Human Exploration Beyond Low-Earth Orbit," AIAA-2015-4456, *AIAA SPACE 2015,* Pasadena, California, 2015.

[3]Perry, J.L., Sargusingh, M.J., and Toomarian, N., "Guiding Requirements for Designing Life Support System Architectures for Crewed Exploration Mission Beyond Low-Earth Orbit," AIAA 2016-5461, *AIAA SPACE 2016,* Long Beach, California, 2016.

[4]Perry, J.L., "Trace Contaminant Control for the International Space Station's Node 1—Analysis, Design, and Verification," NASA TP-218235, April 2017, pp. 32-33.

[5]Carter, L., Kayatin, M., Perry, J., et al. "Design and Delivery of a Filter for Removal of Siloxanes from the ISS Atmosphere," ICES-2016-15, *46th International Conference on Environmental Systems,* Vienna, Austria, 2016.

[6]Perry, J.L., Abney, M.B., Conrad, R.E., et al. "Evaluation of an Atmosphere Revitalization Subsystem for Deep Space Exploration Missions," ICES 2015-107, *45th International Conference on Environmental Systems,* Bellevue, Washington, 2015.

[7]Polanyi, M., "Section III.—theories of the adsorption of gases. A general survey and some additional remarks. Introductory paper to section III," *Transactions of the Faraday Society,* Vol. 28, 1932, pp. 316-333.

[8]Dubinin, M.M., "The potential Theory of Adsorption of Gases and Vapors for Adsorbents with Energetically Nonuniform Surfaces," *Chemical Reviews*, Vol. 60, No. 2, 1960, pp. 235-241.

[9]Olcott, T.M., "Development of a Sorber Trace Contaminant Control System Including Pre- and Post-Sorbers for a Catalytic Oxidizer," NASA CR-2027, Lockheed Missiles and Space Co., Sunnyvale, CA, 1972, p. 26.

[10]Olcott, T.M., "Design, Fabrication, and Test of a Trace Contaminant Control System," NASA CR-147861, Lockheed Missiles and Space Co., Sunnyvale, CA, 1975.

[11]Glasstone, S., *Thermodynamics for Chemists*, New York, D. Van Nostrand Company, Inc., 1947.

[12]Bering, B. P., Dubinin, M. M., and Serpinsky, V. V., "Theory of volume filling for vapor adsorption," *Journal of Colloid and Interface Science*, Vol. 21, No. 4, 1966, pp. 378-393.

[13]Perry, J.L., "Elements of Spacecraft Cabin Air Quality Control," NASA TP-1998-207978, May 1998.

[14]Monje, O., Surma, J.M., Perry, J.L., and Kayatin, M.J., "Measuring Polanyi Potentials for Chemsorb 1000 and Chemsorb 3800," ICES-2016-321*, 46th International Conference on Environmental Systems*, Vienna, Austria, 2016.

[15]Perry, J.L., et al., "Evaluation of an Atmosphere Revitalization Subsystem for Deep Space Exploration Missions," ICES-2015-107, *45th International Conference on Environmental Systems*, Bellevue, Washington, 2015.

[16]Levenspiel, O., *Engineering Flow and Heat Exchange*, New York, Plenum Press, 1998.

[17]Perry, J.L and Kayatin M.J., "Trace Contaminant Control Design Considerations for Enabling Exploration Missions," ICES-2015-108, *45th International Conference on Environmental Systems*, Bellevue, Washington, 2015.

[18]Perry, J.L., "A Users' Guide to the Trace Contaminant Control Simulation Computer Program," NASA TM-108456, April 1994.

[19]Perry, J.L., "Trace Chemical Contaminant Generation Rates for Spacecraft Contamination Control System Design," NASA TM-108497, August 1995.